One-pot aqueous-phase xylose upgrading on Zr-containing BEA zeolites

Elise M. Albuquerque, Priscilla N. Paulino, Renata Sadek, Laetitia Valentin, Jean-Marc Krafft, Stanislaw Dzwigaj, Marco A. Fraga

One-pot aqueous-phase xylose upgrading on Zr-containing BEA zeolites

Elise M. Albuquerque,[1] Priscilla N. Paulino,[1] Renata Sadek,[2] Laetitia Valentin,[2]

Jean-Marc Krafft,[2] Stanislaw Dzwigaj,[2,*] Marco A. Fraga[1,*]

[1]Instituto Nacional de Tecnologia – INT, Laboratório de Catálise, Av. Venezuela, 82/518, Saúde, 20081-312, Rio de Janeiro/RJ, Brazil

[2]Laboratoire de Réactivité de Surface, Sorbonne Université-CNRS, UMR 7197, 4 place Jussieu, 75252, Paris, France

Keywords: hemicellulose; furfuryl alcohol; pentose; lignocellulosic biomass; green chemistry

***Corresponding authors**

Marco André Fraga, E-mail: marco-fraga@int.gov.br, Tel. +552121231152

Stanislaw Dzwigaj, E-mail: stanislaw.dzwigaj@sorbonne-universite.fr, Tel.+33144272113

Abstract

Xylose transformation into furfuryl alcohol was performed over modified BEA zeolites. BEA acidity was modified by incorporating Zr into zeolite by a post-synthesis procedure. HAlBEA showed to be selective towards furfuryl alcohol under reaction conditions used. Zr-containing zeolites were more active than the corresponding BEA catalysts but their efficiency to promote xylose conversion to furfuryl alcohol was related to Zr atoms incorporated in the framework. High Zr loadings generated isolated ZrO_2 which promoted xylose isomerization to xylulose. It was associated with the depletion of Brønsted acid sites since presence of Brønsted and Lewis acid centres are crucial for the cascade process to furfuryl alcohol. ZrHAlBEA catalyst exhibited no significant deactivation upon four reaction cycles. Products distribution was not affected either, indicating that Brønsted and Lewis acid sites are preserved under the reaction conditions. Neither Al nor Zr were leached from the catalysts structure, corroborating their chemical stability in aqueous phase.

1. Introduction

Xylose upgrading to high value-added green chemicals is a strategic approach for waste biomass valorisation since it is one of the major compounds in lignocellulosic biomass along with glucose. This monosaccharide is released in the aqueous phase upon hemicellulose fraction hydrolysis and can thus be converted into any other chemical platform or intermediate. Xylose dehydration to furfural is certainly one of the most studied routes and it has long been performed industrially as furfural production from fossil-based feedstock is not economically competitive [1]. Furfural is actually an important xylose-derivative as it is an intermediate polarity selective solvent [2] and a mid-way chemical feedstock in the production of oxygen-containing heterocycles, such as furfuryl alcohol [3–5] and methylfuran [6–8], and other five-carbon compounds as levulinic acid and alkyl levulinates [9–11]. That is to say that every each of these derivatives may thus be obtained through cascade aqueous-phase reactions starting from xylose at which acid-catalysed xylose dehydration is necessarily the very first reaction step.

Furfuryl alcohol is still industrially the most important chemical obtained from furfural despite all those possibilities. It is produced by gas or liquid phase selective hydrogenation of furfural on metal-based catalysts at high hydrogen pressures (7 – 60 bar) and temperature (130 – 300 ºC). Despite most of the typical hydrogenation metals (Pt, Pd, Ni, Co and Fe) have been applied to this reaction, Cu renders the most active and selective catalysts as this metal favourably hydrogenate C=O group instead of the C=C bonds in the furanic ring [1,12,13]. Nonetheless, the requirement for high hydrogen pressures, the challenge of tuning selectivity and the incidence of deactivation impose the utmost technical hurdles for metal-based systems.

Catalytic transfer hydrogenation, relying on Meerwein–Ponndorf–Verley (MPV) mechanism, is a feasible alternative approach in this regard. It is a highly selective reaction

towards chemo-reduction of carbonyl group, well known to be catalysed by homogeneous Al and Zr alkoxides, which must be present at very high excess in the reaction medium [14]. Heterogeneous systems have long been proved to work as well, particularly acid or base metal oxides [3,12,15–18] and zeolites [19–22]. Furthermore, carbonyl reduction occurs via hydrogen transfer from a H-donor agent, usually an aliphatic alcohol. Choosing a friendly bio-derived alcohol can thus even improve the sustainability of the whole transformation process.

ZrO_2 is one of the most effective catalysts among metal oxides. Monoclinic zirconia was shown to be appreciably more active than its tetragonal polymorph [14]. This trend was not found to be a consequence of a lower activation though, but related to a more appropriate distribution of reactant molecules on the surface of monoclinic structure instead [14]. Different authors [23,24] have concluded that the catalytic activity in MPV reactions is correlated with the number of Lewis acid sites, i.e., tetrahedral Zr^{4+} species. Such correlation was seen to be valid for pure ZrO_2 catalysts as well as ZrO_2-modified oxides, such as ZrO_2/SiO_2, ZrO_2/TiO_2, ZrO_2/CeO_2, ZrO_2/Al_2O_3, ZrO_2/Ga_2O_3 and ZrO_2/In_2O_3 [23,24]. Furthermore, it has been claimed that stronger Lewis acid sites are more effective to promote MPV reactions [25–27]. Brønsted acid sites, on the other side, have been proved to have no participation in the reaction [27] despite some previous debate suggesting otherwise [28,29].

Zr-modified zeolites have also been studied on MPV reductions, most of them relaying on beta structure. Such catalysts showed high performance for producing levulinic acid/alkyl levulinates and γ-valerolactone from furfural [9,30], which involves one or two MPV reduction steps – furfural to furfuryl alcohol and levulinic acid/levulinate to γ-valerolactone. Conversely, Zr-substituted zeolite beta was found less active than Hf-containing ones towards furfuryl alcohol [22]. Anyway, zeolite beta modified with tetravalent metals (Ti^{4+}, Sn^{4+}, Zr^{4+} and Hf^{4+}) has been generally reported to promote MPV

reduction [14,26,31–35]. Nonetheless, different activity orders have been established according to the molecule holding the carbonyl group, such as furfural [22], alkyl cyclohexanones [31,33,36], benzaldehyde [36], cynamaldehyde and other branched α,β-unsaturated aldehydes [32]. These reports reveal that catalytic activity prediction is not a simple, straightforward task.

One-pot conversion of xylose to furfuryl alcohol, at which xylose dehydration step is followed by furfural hydrogenation, have recently been reported through different pathways relying on a conventional metal-catalyzed hydrogenation [37–40] or via MPV reduction [3,41–44]. Each route requires a very distinct catalytic system, either a bifunctional acid/metal catalyst [37,40] or Brønsted/Lewis acid catalysts [41,42]. Indeed, we have previously reported that furfuryl alcohol yields of ~80% can be accomplished over beta zeolite while a much poorer performance was observed on USY, rendering only ~35% yield [41].

In this work, the surface acidity of beta zeolite was modified by the incorporation of Zr atoms into the zeolite by a two-step post-synthesis procedure. The surface reactivity for straightforward xylose upgrading to furfuryl alcohol was then investigated. Particular attention was given to the aqueous-phase processing, considering that pentoses are made available in large amounts of water as a side-stream from waste biomass pretreatment. Such approach aims at contributing to the integration of green chemicals and biofuels processes in a lignocellulosic biorefinery concept.

2. Experimental

2.1. Catalysts synthesis

Dealumination of a tetraethylammonium beta (TEABEA) zeolite with a Si/Al atomic ratio of 14 was performed by a treatment with nitric acid solution (13 mol L^{-1}) at 80 °C for 4

h in order to obtain a siliceous BEA zeolite with Si/Al atomic ratio of 1000. After that, the solid was washed several times with distilled water and dried at 95 °C overnight, resulting a dealuminated BEA zeolite labelled as SiBEA.

Zirconium incorporation was carried out by adding SiBEA sample to a solution of $Zr(NO_3)_4.4H_2O$ (Chemical Point Deisenhafen Company, Germany) maintained at pH = 2.6 in a concentration to lead to either 3 wt% or 6 wt% of zirconium in the final catalysts. The suspensions were stirred for 24 h at room temperature and then the solids were separated in a rotary evaporator under vacuum, and then dried for 2 h at 60 °C. Samples were named as Zr_xSiBEA where *x* stands for the nominal Zr loading.

Two other samples were also obtained by incorporating Zr into a HAlBEA following the same procedure and named as Zr_xHAlBEA accordingly. The HAlBEA was obtained by calcination of TEABEA zeolite at 550 °C for 15 h.

2.2. Physicochemical characterization

Samples structure was assessed by X-ray powder diffraction (XRD) using a Bruker D8 Advance diffractometer with CuKα radiation and equipped with a Lynx-eye position sensitive detector. Diffractograms were collected with a scan rate of 3° min^{-1} in the 2θ Bragg range of 10-90°.

Zeolite chemical composition was determined by inductively coupled plasma optical emission spectroscopy (ICP-OES) using a Varian Vista MXP spectrometer. Previously to ICP-OES analyses, the zeolites were calcined at 900 °C for 6 h and then dissolved in a mixture of HNO_3 (65%) and HF (40%) using a Milestone Ethos 1 digester. All solutions were analysed in triplicate and presented a standard deviation <5 %.

DR UV–vis spectra of as prepared Zr_xHAlBEA and Zr_xSiBEA were recorded at ambient atmosphere on a Cary 5000 Varian spectrometer equipped with a double integrator with polytetrafluoroethylene as reference.

Acidic properties of all samples were assessed by adsorption of pyridine (Py) and CO followed by infrared spectroscopy. Before analysis, samples were pressed at ~1 ton cm^{-2} into thin wafers of ca. 10 mg cm^{-2} and placed inside an infrared cell. Prior to pyridine adsorption/desorption experiments, the wafers were activated by calcination in static conditions at 450 °C for 3 h in O_2 ($1.6\ 10^4$ Pa) and outgassed at 300 °C (10^{-3} Pa) for 1 h. Subsequently, pyridine was introduced (133 Pa) into the cell at room temperature. The IR spectra were collected on a Bruker Vector 22 spectrometer (resolution 2 cm^{-1}, 128 scans) after outgassing at 150 °C for 1 h. The resulting spectra were obtained after subtraction of the spectrum recorded before pyridine adsorption. The quantification of acid sites was carried out as reported by Emeis [45].

As for CO adsorption experiments, the wafers firstly were calcined at 450 °C for 2 h in flowing 2.5 % O_2/Ar and then outgassed at 300 °C (10^{-3} Pa) for 1 h. After thermal treatment, the samples were cooled down to -173 °C. CO was introduced in the cell until it reached an equilibrium pressure of 133 Pa. Gradual evacuation was then performed in dynamic vacuum at -173 °C.

2.3. Catalytic activity

Aqueous-phase xylose reaction was performed under inert atmosphere in a semi-batch stainless steel PARR reactor. In a typical experiment, the reactor was loaded with a xylose solution (83 mmol L^{-1}) prepared in water:2-propanol (1:1) and 0.25 g of catalyst, following the same reaction conditions reported elsewhere [41]. After sealing and purging with N_2, the temperature was raised to 130 °C and the system pressure adjusted to 30 bar while stirring speed was set at 600 rpm. Under these reaction conditions the absence of

diffusion limitations could be ensured [37,39,40]. The beginning of the reaction was considered as soon as the temperature was reached and it was then carried out and monitored for 6 h. Liquid samples were taken at regular times and analysed by high performance liquid chromatography (HPLC) in a Waters Alliance e2695 liquid chromatograph equipped with a photodiode array detector 2998 (PDA) and a refractive index detector 2414 (RID), which was set at 50 °C. All chemicals were separated in a Biorad Aminex HPX-87H ion exchange column set at 65 °C using a sulphuric acid aqueous solution at 5 mmol L^{-1} as mobile phase at 0.7 mL min^{-1} in an isocratic mode. Prior to HPLC analyses, liquid samples were filtered with a polyethylene 0.22 µm filter.

Xylose conversion (X) and product distribution (S) were calculated along reaction time (*t*) on a molar basis by the following equations:

$$X\ (\%) = \frac{mols\ of\ xylose\ in\ the\ beginning - mols\ of\ xylose\ at\ t}{mols\ of\ xylose\ in\ the\ beginning}\ x\ 100$$

$$S\ (mol\%) = \frac{mols\ of\ product\ at\ t}{mols\ of\ xylose\ consumed\ at\ t}\ x\ 100$$

Reusability tests were also performed using the dried spent catalysts. Four consecutive reaction cycles were carried out using a new xylose solution prepared in water:2-propanol (1:1). Reaction conditions were kept exactly the same (130 ºC, 30 bar N_2, 600 rpm).

2.4. Characterization of spent catalysts

After reaction, catalysts were recovered by filtration, washed with water and dried before complementary characterization analyses were performed to assess their chemical

stability. The spent samples were examined by ICP-OES following the same analyses conditions described hereinbefore.

3. Results and discussion

The structure of all synthesized samples and the incorporation of Zr were firstly investigated to ensure the catalysts hold the physicochemical features initially designed for the direct conversion of xylose in water. XRD patterns were consistent with the formation of pure and well-crystallized BEA zeolites (Figure S1), evidencing that the thermal treatment, dealumination in nitric acid solution and Zr incorporation did not affect samples crystallinity, and BEA structure did not collapse in line with what was reported elsewhere [46,47]. No crystalline phases of ZrO_2 were detected in any of the Zr-containing zeolites, suggesting the formation of quite well dispersed phases or the Zr incorporation in the zeolite framework, in agreement with earlier reports [47,48].

Chemical analysis performed by inductively coupled plasma optical emission spectroscopy (ICP-OES) allowed to obtain Al and Zr contents and determine Si/Al and Si/Zr ratios. The actual Zr content was indeed quite similar to the aimed nominal ones as summarized in Table 1. Theses samples allow investigating two distinct families of zeolites holding practically the same Zr loadings.

To evaluate the Zr coordination state in Zr-based catalysts, DR UV-vis analysis was performed, and the spectra are presented in Figure 1. No feature characteristics of d-d transitions were displayed in the visible range above 400 nm in the electronic spectrum of all samples, suggesting the d^0 configuration of the Zr^{4+} ions, in agreement with earlier report [49]. Zr_3SiBEA, Zr_6SiBEA, Zr_3HAlBEA and Zr_6HAlBEA samples exhibited a band within 208-228 nm related to the charge transfer between O^{2-} and Zr^{4+} ions in a tetrahedral coordination [46,47,50,51]. All materials presented additional bands at 250-350 nm related

to the metal-to-ligand charge transition of Zr-O-Zr in ZrO_2, in agreement with Haskouri *et al* [52]. Therefore, these results indicate a contribution of bulk ZrO_2 in all synthesized catalysts. In summary, UV-Vis results showed that in all Zr-containing BEA samples both Zr ions in the zeolite framework and bulk oxide occurred.

FTIR spectra collected right after *in situ* pretreatment and before contacting the samples with any probe molecule were analysed to bring some insight into the Al removal and the incorporation of Zr into BEA framework (Figure 2). The spectrum of HAlBEA sample exhibited bands attributed to AlO-H groups at 3781 and 3667 cm^{-1}, bridging acidic hydroxyls Si-O(H)-Al at 3616 cm^{-1} [55], isolated external SiO-H groups as a narrow band at 3747 cm^{-1}, isolated internal SiO-H groups at 3741 cm^{-1}, isolated terminal SiO-H groups at 3716 cm^{-1} and H-bonded SiO-H at 3520 cm^{-1} [50,54–56]. The incorporation of zirconium ions in HAlBEA led to almost total disappearance of the bands at 3781, 3667 and 3616 cm^{-1}, implying that zirconium ions is interacting with AlO-H groups and bridging acidic hydroxyls Si-O(H)-Al groups. On the other hand, the bands related to isolated external SiO-H groups at 3749 cm^{-1}, and isolated terminal SiO-H groups at 3724 cm^{-1} remained, while new bands were observed at 3795, 3763 and 3700-3665 cm^{-1}. The former two bands (3795 and 3763 cm^{-1}) are associated with extra-framework Zr-OH groups, in agreement with what was observed by UV-Vis analysis while the latter ones (3700-3665 cm^{-1}) are attributed to open $Zr(OSi)_3OH$ sites [57].

The elimination of aluminium atoms from BEA zeolite framework, after treatment with HNO_3 solution, was evidenced by the disappearance of the bands related to AlO-H at 3781 and 3667 cm^{-1} and bridging acidic hydroxyls Si-O(H)-Al groups at 3616 cm^{-1} as can be seen in Figure 2, in agreement with earlier investigations [56,58]. At the same time, the appearance of bands at 3738 cm^{-1}, associated to isolated silanol groups, 3713 cm^{-1}, related to isolated terminal SiO-H groups, and a broad intense band at 3512 cm^{-1}, due to H-bonded

SiOH groups, reveals the creation of important amounts of vacant T-atom sites in SiBEA zeolite [58]. The introduction of zirconium in SiBEA led to almost total disappearance of the bands at 3738 and 3713 cm^{-1} attributed to isolated and terminal silanol groups, respectively, and the band at 3512 cm^{-1} associated with H-bonded SiOH groups. At the same time, the emergence of a band at 3677 cm^{-1} attributed to $Zr(OSi)_3OH$ open sites could be noticed, in line with earlier report [57].

After the *in situ* pretreatment, adsorption of pyridine (Py) and CO as probe molecules was performed to determine the nature and strength of acidic centres in the zeolites. As expected, FTIR-Py spectrum of SiBEA catalyst confirmed that this sample did not present any acidity (Figure 3 and Table 1). The incorporation of low amounts of zirconium into SiBEA led to the formation of moderate Lewis acidic centers in Zr_3SiBEA, evidenced by the appearance of bands at 1610 and 1446 cm^{-1} (Figure 3) due to pyridine bonded to isolated zirconium (IV) species, probably present in the zeolite framework [58]. No similar bands were observed for Zr_6SiBEA, only the one related to physiosorbed pyridine at 1442 cm^{-1}, which might be associated with the higher amount of extra-framework Zr moieties (ZrO_2) in this high Zr-loading sample. As for HAlBEA, typical pyridinium ions bands were seen at 1545 and 1637 cm^{-1}, indicating the presence of Brønsted acid sites related to the acidic proton of Al–O(H)–Si groups, in line with earlier data on similar solids [53,58]. The bands at 1450 and 1620 cm^{-1} correspond to pyridine interacting with strong Lewis acidic centres (Al^{3+}) while the one at 1610 cm^{-1} is associated with pyridine interacting with moderate Lewis acidic centres. The absorption at 1490 cm^{-1} corresponds to pyridine interacting with both Brønsted and Lewis acid sites. Additionally, the presence of a small band at around 1576 cm^{-1} may be associated with pyridine coordinately bonded to weak Lewis acid sites [59]. All those absorption bands (1637, 1620, 1545, 1490 and 1450 cm^{-1}) were still recorded after addition of zirconium to HAlBEA. However, such modification in the zeolite composition

consistently dropped the amount of Brønsted and Lewis acid sites in both Zr_3HAlBEA and Zr_6HAlBEA (Table 1). This might be related to some degree of ion exchange occurred between the proton of bridging hydroxyls Si-O(H)-Al with zirconium species.

FTIR spectroscopy of adsorbed CO can also be used to dose the acidity of different catalysts [59,62]. Figure 4 presents the difference spectra obtained, in the OH vibration region, after CO adsorption at -173 °C. CO adsorption forms hydrogen bonds with Brønsted acid sites, which leads to a broadening and a red shift of the corresponding OH bands. The higher the strength of Brønsted acid sites, the larger the shift of the OH modes [60,61]. As can be observed for HAlBEA, the introduction of CO at -173 °C led to the appearance of bands at 3648, 3585, 3445 and 3297 cm^{-1} and negative bands at 3782, 3740, 3670 and 3618 cm^{-1} (Figure 4). The shifts of 92 cm^{-1} observed for isolated external SiO-H groups and of 130 cm^{-1} observed for terminal internal SiO-H groups indicate the weak acidic character of those two silanol groups. The bands related to AlO-H and Al-O(H)-Si groups were red shifted to 3445 and 3297 cm^{-1}. Al-O(H)-Si groups frequency shift of 319 cm^{-1} demonstrates the strong acid character of the proton of these groups (Figure 4). Moreover, the band at 3445 cm^{-1} seems to be related to perturbed extra-framework AlO-H groups and the shift of 222 cm^{-1} suggests medium acidic character, in line with previous work of Hadjiivanov [55]. In the case of Zr_6HAlBEA, the absence of bands at 3445 and 3297 cm^{-1} (Figure 4) suggests that Al-OH and Al-O(H)-Si groups have been consumed during Zr incorporation procedure. Two broad bands were recorded at 3650 and 3583 cm^{-1} as a consequence of the red shift of isolated external and internal SiO-H groups frequencies (initially at 3748 and 3724 cm^{-1}), respectively. The shifts values of 98 cm^{-1} for isolated external SiO-H groups and of 141 cm^{-1} for isolated internal SiO-H groups indicate that both Si-OH groups have weak acidic character.

As for siliceous SiBEA zeolite, bands at 3640, 3600, 3430 and 3301 cm^{-1} and negative bands at 3739 and 3715 cm^{-1} were registered (Figure 4). Similarly, the shifts observed for isolated internal (98 cm^{-1}) and terminal internal Si-OH (113 cm^{-1}) indicate that both silanol groups have a weak acidity. The very low intensity of bands at 3430 and 3301 cm^{-1} suggests a poor content of Al-OH and Al-O(H)-Si groups, as expected. With respect to Zr_6SiBEA, two bands were seen at 3650 and 3588 cm^{-1} and three negative bands at 3797, 3748 and 3717 cm^{-1}. This catalyst also presented weak acid silanol groups as evidenced by the red shift of 98 cm^{-1} for isolated internal silanol (from 3748 to 3650 cm^{-1}) and of 129 cm^{-1} for isolated terminal silanol (from 3717 to 3588 cm^{-1}). These findings are in line with pyridine adsorption, which revealed that Zr_6SiBEA zeolite did not show Brønsted acidity.

When CO is adsorbed at low temperatures (~-173 °C) it coordinates to Lewis acid sites through sigma donation and as consequence of those interactions, the vibration modes of the adsorbed CO is shifted to higher frequencies in relation to the reference band of pseudoliquid CO at 2138 cm^{-1} [57]. The spectra obtained after CO adsorption in the region of carbonyl vibration mode are shown in Figure 5. Under CO equilibrium pressure of 100 Pa, carbonyl bands are detected at 2215, 2192, 2172, 2156 and 2140 cm^{-1} in the spectrum of HAlBEA (Figure 5, spectrum a). The band at 2140 cm^{-1} is assigned to physisorbed CO which indeed vanishes first upon outgassing as observed in the sequential spectra (Figure 5b-f). The band at 2156 cm^{-1} also disappears upon outgassing at the same time that the band at 3648 cm^{-1} (Figure 4), being then assigned to the stretching of CO bonded to silanol groups, as reported earlier [62]. Further outgassing this sample leads to the decay of intensity of the band at 2172 cm^{-1} (Figure 5, spectra b-f), what is typical of CO interacting with bridging zeolite hydroxyls (Al-O(H)-Si), the Brønsted acid sites. Extra-framework Al sites (Lewis acid sites) were shown to be present in HAlBEA by carbonyl bands at 2192 and 2215 cm^{-1} [60]. By adding high amount of Zr into this sample (Zr_6HAlBEA), CO adsorption bands

appear at 2141 and 2167 cm^{-1} (Figure 5). The former is due to physisorbed CO as assigned hereinbefore. As for the latter band, its intensity reduces together with the OH band at 3583 cm^{-1} (Figure 4), suggesting it can be associated with to the formation of OH···CO complexes on open $Zr(OSi)_3OH$ sites as reported elsewhere [57]. Comparing the position of the band related to the $Zr(OSi)_3OH$ open sites (2167 cm^{-1}) with the ones related to the CO interacting with HAlBEA Brønsted acid sites (2174 cm^{-1}) and with silanol groups (2150 cm^{-1}), it is possible to infer on the weak acidity of the respective OH groups [57]. Upon further outgassing at higher dynamic vacuum, a band at 2177 cm^{-1} showed up, which could correspond to the interaction of CO with Lewis acid sites, related to the closed ($Zr(OSi)_4$) sites, in agreement with earlier report of Ivanova *et al*. [57].

The adsorbed CO spectrum of SiBEA sample exhibited two main carbonyl bands at 2158 and 2139 cm^{-1} (Figure 5). Once again the presence of physisorbed CO is observed by the band at ~2140 cm^{-1} while the band at 2158 cm^{-1} can be ascribed to CO interacting with internal silanol groups of the vacant T-atom sites, confirming the presence of those sites in SiBEA catalyst. Addition of Zr into this sample led to the appearance of a carbonyl band at 2167 cm^{-1} in the Zr_6SiBEA spectrum, which is similarly associated with the formation of OH···CO complexes on open Zr sites [57]. In the same way that was observed for Zr_6HAlBEA, Zr_6SiBEA presented a band at 2177 cm^{-1} related to the presence of close Zr sites [57].

All zeolites were tested in liquid-phase xylose transformation under mass-transfer free conditions and the evolution of conversion as a function of reaction time is depicted in Figure 6. Considering that a large volume of water is present in the hydrolysis of hemicellulose fraction in waste biomass, all catalytic activity was performed the presence of high amounts of water.

Most zeolites showed to be active for xylose conversion. Siliceous SiBEA catalyst, however, barely reached 7% conversion after 6-h reaction, indicating its low activity. As a matter of fact, this performance is fairly similar to that observed in a control experiment at which no catalyst was used. It thus reveals that siliceous SiBEA is not active towards xylose conversion, which can be associated with its expected lack of acidity evidenced by the infrared spectroscopy experiments discussed hereinbefore. This result is consistent with the previously reported behaviour of SiO_2 [39,42].

Adding Zr into SiBEA zeolite led to a substantial improvement in catalytic activity reaching xylose conversion of around 35% after 6 h of reaction (Figure 6). Such an impact is credited to the weak Lewis acidity generated by Zr species as disclosed by infrared spectra using CO and pyridine as probe molecules (Figure 3). The amount of Zr fetched no meaningful influence on activity though. As revealed by UV-vis spectroscopy (Figure 1), these samples hold mainly framework Zr^{4+} sites and well dispersed ZrO_2 moieties. Therefore, these results are likely related to the high activity of ZrO_2 as disclosed by the control experiment ran with a commercial bulk ZrO_2 depicted in Figure S2a. The time-conversion curves of Zr_xSiBEA catalysts are also graphed along with ZrO_2 results for the sake of comparison.

This discussion on the catalyst behaviour is corroborated by the product distribution displayed in Figure 7. Isomerization of xylose to xylulose (Scheme 1) was the leading reaction over both Zr_xSiBEA catalysts, with a surprisingly minor production of other furanic compounds with selectivities below 10%. The tiny formation of furfuryl alcohol was further supressed when Zr loading in SiBEA increased. Indeed, Lewis acid sites, the only ones present on Zr_xSiBEA, are known to be responsible for the predominant isomerization of xylose to xylulose [39,40,63]. A similar behaviour was observed in the control experiment with bulk ZrO_2 catalyst (Figure S2b), at which xylulose was the main product.

The absence of Brønsted acid sites on Zr_xSiBEA catalysts explains the low activity for dehydration of pentoses into furfural, hampering the cascade reaction illustrated in Scheme 1 towards other furanic compounds. The small amounts of such chemicals could be associated with the weak acid sites from extra-framework Zr species, which has been reckoned as being able to catalyse the acid driven reaction [30]. This way, the furfural produced is sequentially transformed into furfuryl alcohol. It should be mentioned though that these compounds were also formed over bulk ZrO_2 used in the control experiment (Figure S3). Therefore, the contribution of xylose/xylulose dehydration over ZrO_2 Lewis acid sites on Zr_xSiBEA surface allowing the transformation up to furfuryl alcohol should not be totally disregarded. Though kinetically slow, monosaccharide dehydration has indeed been reported to occur on Lewis sites [63].

It should lastly be highlighted that even though many studies have focused on beta zeolites at which Al was substituted with Zr by post-synthetic methods [19,20,25,46,47,50,51,56], i.e. dealumination followed by impregnation in a similar protocol used herein, these materials have rarely been used in liquid-phase reactions starting from xylose [19]. Indeed, they are mostly focused on the transformation of furfural [20,47].

The collection of Al-containing BEA catalysts was also active in xylose transformation (Figure 6). Similarly, introducing Zr into HAlBEA enhanced global activity, but in these samples increasing Zr content further increased catalytic activity. Due to the multiple possible reactions in xylose cascade conversion (Scheme 1), the behaviour of these catalysts must be discussed on the basis of their product distribution (Figure 8). Indeed, the distribution of products obtained from xylose was very sensitive to the acidity tailored by the chemical composition of these catalysts. Even though xylulose, furfural and furfuryl alcohol were the main products obtained, their selectivity varied appreciably.

Furfuryl alcohol was undeniably the main product on HAlBEA (Figure 8a), reaching selectivity of around 80%. These results are in line with previous report on the performance of a commercial beta zeolite [41]. Despite being in a lower level (selectivity of ~35%), furfuryl alcohol was also majorly produced over Zr_3HAlBEA while xylulose was practically the only product on the zeolite with the highest Zr loading (Zr_6HBEA). These findings, along with the results obtained with Zr_xSiBEA catalysts family, indicate that the tandem conversion of xylose to furfuryl alcohol is only promoted when both Lewis and Brønsted are present in zeolite catalysts as assessed by infrared spectroscopy of adsorbed probe molecules. Introducing increasing amounts of Zr into initial HAlBEA catalyst led to an increasing generation of weak Lewis acid sites in detriment of Brønsted ones (Table 1). Once Brønsted acidity is depleted, dehydration step cannot occur, the cascade reactions are stopped and, as a consequence, no furfuryl alcohol is formed (Figure 8).

The vital role played by the existence of both Brønsted and Lewis sites on beta zeolites were also reported elsewhere [19,30]. However, in such previous reports, the cascade reaction was pushed further, allowing the formation of γ-valerolactone. For that to occur, furfuryl alcohol is hydrolysed to levulinic acid/alkyl levulinates on Brønsted acid sites, and these compounds are then finally MPV hydrogenated to γ-valerolactone on Lewis acid sites. A simplified scheme of these cascade reactions can be found in Scheme S1. It should be considered that harsher conditions were used when compared to the ones applied in this present work, particularly higher temperature (170 ^{o}C versus 130 ^{o}C herein) and longer reaction time (24 – 48 h versus 6 h herein). It is indeed reckoned that higher temperatures allow the cascade process to accelerate [30,42]. Another very important issue to be taken into account is that in this present contribution a large amount of water was used in the reaction medium (water:2-propanol 1:1 versus pure 2-propanol elsewhere [19,30]) since the main focus here is the upgrade of waste lignocellulosic biomass hydrolysates, which is a

low-concentration xylose aqueous solution. The presence of water is well known to hinder MPV mechanism [3,41,42] and it is thus conceivable that the reaction was limited to furfuryl alcohol formation (Scheme S1).

Carbon balance was seen to slightly drop along reaction (Figure 7), but it was always ≥90% when all C5 products were accounted as quantified by HPLC. Minor by-products detected on some catalysts were identified as retro aldol condensation products (C3 and C2) but they were not considered to determine the time-dependent carbon balance curves. No acetals or products resulting from etherification reactions between furfuryl alcohol, 2-propanol or furfuryl alcohol/2-propanol molecules were identified.

These results reported herein show that acidic BEA zeolite catalyst can promote xylose dehydration to furfural followed by its transfer hydrogenation with the aid of *in situ* hydrogen generation by 2-propanol. Propanone was indeed detected in these catalytic runs, evidencing the oxidation of 2-propanol through MPV mechanism as reported before on a commercial beta zeolite [41] and [Al]-SBA-15 mesoporous catalyst [42]. It is proposed that the reaction mechanism starts by xylose isomerization to xylulose over Lewis acid sites. Xylose and xylulose both can be dehydrated over Brønsted acid sites to furfural, though, it seems that xylulose dehydration is the preferred step. Furfural is then coordinated to Lewis acid sites through a six membered ring [41] and hydrogenated by the alkoxide species that were generated by the 2-propanol adsorption.

To assess the recyclability of the catalysts, Zr_3HAlBEA, which disclosed the best performance within the one containing Zr, was recovered, dried and used in consecutive reaction runs always using a new starting xylose aqueous solution. Figure 9 presents the results obtained for xylose conversion and products selectivities after 6 h of reaction. Xylose average conversion was around 20% and no significant deactivation was observed. Products

distribution showed to not be affected, indicating that both Brønsted and Lewis acid sites are still active after four consecutive runs.

Finally, chemical composition analysis of spent Zr_3HAlBEA and Zr_6HAlBEA revealed that neither Al or Zr are leached from catalysts structure in close agreement with the catalyst performance after consecutive reaction tests. Indeed, ICP-OES results showed that Zr_3HAlBEA contained 2.9 wt% and 3.2 wt% of Al and Zr, respectively, while Zr_6HAlBEA presented 3.0 wt% and 6.3 wt% of Al and Zr, which are very comparable with those data collected from the fresh samples (Table 1).

4. Conclusion

The results presented herein showed that metal-free BEA-based catalysts are potential catalyst to promote the direct conversion of xylose into furfuryl alcohol through a molecular hydrogen free system. Zr-based SiBEA catalysts were able to promote xylose isomerization to xylulose, though, they were not effective to proceed the sequential reaction step, forming only small amount of the furanic compounds, due to the lack of Brønsted acid sites on these samples. The presence of Al atoms on BEA framework (HAlBEA) led to a highly furfuryl alcohol selective catalyst. Although the addition of Zr into HAlBEA catalyst increased catalytic activity, furfuryl alcohol selectivity decreased. This behaviour was shown to be associated with the acidity type (Brønsted or Lewis acid sites) and balance of acid sites on the catalyst surface. The presence of both Brønsted and Lewis acid centres are crucial for the cascade process to proceed.

Acknowledgements

Authors acknowledge financial support from CNPq and FAPERJ. PNP (Proc. 312810/ 2016-4) and EMA (Proc. 313014/ 2016-7) thank PCI/CNPq for their post-doctoral grants.

References

[1] R. Mariscal, P. Maireles-Torres, M. Ojeda, I. Sádaba, M. López Granados

Furfural: A renewable and versatile platform molecule for the synthesis of chemicals and fuels

Energy Environ. Sci. 9 (2016) 1144–1189.

[2] K.J. Zeitsch

The chemistry and technology of furfural and its many by-products

Volume 13, 2000.

[3] R. López-Asensio, J.A. Cecilia, C.P. Jiménez-Gómez, C. García-Sancho, R. Moreno-Tost, P. Maireles-Torres

Selective production of furfuryl alcohol from furfural by catalytic transfer hydrogenation over commercial aluminas

Appl. Catal. A Gen. 556 (2018) 1–9.

[4] X. Chen, L. Zhang, B. Zhang, X. Guo, X. Mu

Highly selective hydrogenation of furfural to furfuryl alcohol over Pt nanoparticles supported on g-C_3N_4 nanosheets catalysts in water

Sci. Rep. 6 (2016) 1–13.

[5] M.J. Taylor, L.J. Durndell, M.A. Isaacs, C.M.A. Parlett, K. Wilson, A.F. Lee, G. Kyriakou

Highly selective hydrogenation of furfural over supported Pt nanoparticles under mild conditions

Appl. Catal. B Environ. 180 (2016) 580–585.

[6] F. Dong, G. Ding, H. Zheng, X. Xiang, L. Chen, Y. Zhu, Y. Li

Highly dispersed Cu nanoparticles as an efficient catalyst for the synthesis of the biofuel 2-methylfuran

Catal. Sci. Technol. 6 (2016) 767–779.

[7] S. Srivastava, G.C. Jadeja, J. Parikh

A versatile bi-metallic copper-cobalt catalyst for liquid phase hydrogenation of furfural to 2-methylfuran

RSC Adv. 6 (2016) 1649–1658.

[8] N.S. Date, A.M. Hengne, K.W. Huang, R.C. Chikate, C. V. Rode

Single pot selective hydrogenation of furfural to 2-methylfuran over carbon supported iridium catalysts

Green Chem. 20 (2018) 2027–2037.

[9] M.M. Antunes, S. Lima, P. Neves, A.L. Magalhães, E. Fazio, A. Fernandes, F. Neri, C.M. Silva, S.M. Rocha, M.F. Ribeiro, M. Pillinger, A. Urakawa, A.A. Valente

One-pot conversion of furfural to useful bio-products in the presence of a Sn,Al-containing zeolite beta catalyst prepared via post-synthesis routes

J. Catal. 329 (2015) 522–537.

[10] X. Hu, S. Jiang, L. Wu, S. Wang, C.Z. Li

One-pot conversion of biomass-derived xylose and furfural into levulinate esters via acid catalysis

Chem. Commun. 53 (2017) 2938–2941.

[11] C. Fang, Y. Liu, W. Wu, H. Li, Z. Wang, W. Zhao, T. Yang, S. Yang

One pot cascade conversion of bio-based furfural to levulinic acid with Cu-doped niobium phosphate catalysts

Waste and Biomass Valori. 10 (2019) 1141–1150.

[12] L. Grazia, A. Lolli, F. Folco, Y. Zhang, S. Albonetti, F. Cavani

Gas-phase cascade upgrading of furfural to 2-methylfuran using methanol as a H-transfer reactant and MgO based catalysts

Catal. Sci. Technol. 6 (2016) 4418–4427.

[13] K.L. Deutsch, B.H. Shanks

Active species of copper chromite catalyst in C-O hydrogenolysis of 5-methylfurfuryl alcohol

J. Catal. 285 (2012) 235–241.

[14] F. Gonell, M. Boronat, A. Corma

Structure-reactivity relationship in isolated Zr sites present in Zr-zeolite and ZrO_2 for the Meerwein-Ponndorf-Verley reaction

Catal. Sci. Technol. 7 (2017) 2865–2873.

[15] F. Wang, N. Ta, W. Shen

MgO nanosheets, nanodisks, and nanofibers for the Meerwein-Ponndorf-Verley reaction

Appl. Catal. A Gen. 475 (2014) 76–81.

[16] R.S. Assary, L.A. Curtiss, J.A. Dumesic

Exploring Meerwein-Ponndorf-Verley reduction chemistry for biomass catalysis using a first-principles approach

ACS Catal. 3 (2013) 2694–2704.

[17] J. Zhang, K. Dong, W. Luo, H. Guan

Selective transfer hydrogenation of furfural into furfuryl alcohol on Zr-containing catalysts using lower alcohols as hydrogen donors

ACS Omega. 3 (2018) 6206–6216.

[18] X. Tang, L. Hu, Y. Sun, G. Zhao, W. Hao, L. Lin

Conversion of biomass-derived ethyl levulinate into γ-valerolactone via hydrogen transfer from supercritical ethanol over a ZrO_2 catalyst

RSC Adv. 3 (2013) 10277–10284.

[19] J.A. Melero, G. Morales, J. Iglesias, M. Paniagua, C. López-Aguado, K. Wilson, A. Osatiashtiani, **Efficient one-pot production of γ-valerolactone from xylose over Zr-Al-Beta zeolite: Rational optimization of catalyst synthesis and reaction conditions**

Green Chem. 19 (2017) 5114–5121.

[20] S. Song, L. Di, G. Wu, W. Dai, N. Guan, L. Li

Meso-Zr-Al-beta zeolite as a robust catalyst for cascade reactions in biomass valorization

Appl. Catal. B Environ. 205 (2017) 393–403.

[21] L. Bui, H. Luo, W.R. Gunther, Y. Román-Leshkov

Domino reaction catalyzed by zeolites with Brønsted and Lewis acid sites for the production of γ-valerolactone from furfural

Angew. Chemie Int. Ed. 52 (2013) 8022–8025.

[22] M. Koehle, R.F. Lobo

Lewis acidic zeolite Beta catalyst for the Meerwein-Ponndorf-Verley reduction of furfural

Catal. Sci. Technol. 6 (2016) 3018–3026.

[23] V.L. Sushkevich, I.I. Ivanova, S. Tolborg, E. Taarning

Meerwein-Ponndorf-Verley-Oppenauer reaction of crotonaldehyde with ethanol over Zr-containing catalysts

J. Catal. 316 (2014) 121–129.

[24] J.F. Miñambres, M.A. Aramendía, A. Marinas, J.M. Marinas, F.J. Urbano

Liquid and gas-phase Meerwein-Ponndorf-Verley reduction of crotonaldehyde on ZrO_2 catalysts modified with Al_2O_3, Ga_2O_3 and In_2O_3

J. Mol. Catal. A Chem. 338 (2011) 121–129.

[25] J. Wang, K. Okumura, S. Jaenicke, G.K. Chuah

Post-synthesized zirconium-containing Beta zeolite in Meerwein-Ponndorf-Verley reduction: Pros and cons

Appl. Catal. A Gen. 493 (2015) 112–120.

[26] J. Wang, S. Jaenicke, G.K. Chuah

Zirconium-Beta zeolite as a robust catalyst for the transformation of levulinic acid to γ-valerolactone via Meerwein-Ponndorf-Verley reduction

RSC Adv. 4 (2014) 13481–13489.

[27] Z.K. Gao, Y.C. Hong, Z. Hu, B.Q. Xu

Transfer hydrogenation of cinnamaldehyde with 2-propanol on Al_2O_3 and SiO_2-Al_2O_3 catalysts: Role of Lewis and Brønsted acidic sites

Catal. Sci. Technol. 7 (2017) 4511–4519.

[28] F.J. Urbano, M.A. Aramendía, A. Marinas, J.M. Marinas

An insight into the Meerwein-Ponndorf-Verley reduction of α,β-unsaturated carbonyl compounds: Tuning the acid-base properties of modified zirconia catalysts

J. Catal. 268 (2009) 79–88.

[29] S. Axpuac, M.A. Aramendía, J. Hidalgo-Carrillo, A. Marinas, J.M. Marinas, V. Montes-Jiménez, F.J. Urbano, V. Borau

Study of structure-performance relationships in Meerwein-Ponndorf-Verley reduction of crotonaldehyde on several magnesium and zirconium-based systems

Catal. Today. 187 (2012) 183–190.

[30] B. Hernández, J. Iglesias, G. Morales, M. Paniagua, C. López-Aguado, J.L. García Fierro, P. Wolf, I. Hermans, J.A. Melero

One-pot cascade transformation of xylose into γ-valerolactone (GVL) over

bifunctional Brønsted-Lewis Zr-Al-beta zeolite

Green Chem. 18 (2016) 5777–5781.

[31] Y. Zhu, G. Chuah, S. Jaenicke

Chemo- and regioselective Meerwein-Ponndorf-Verley and Oppenauer reactions catalyzed by Al-free Zr-zeolite beta

J. Catal. 227 (2004) 1–10.

[32] Y. Zhu, G.K. Chuah, S. Jaenicke

Selective Meerwein-Ponndorf-Verley reduction of α, β-unsaturated aldehydes over Zr-zeolite beta

J. Catal. 241 (2006) 25–33.

[33] A. Corma, M.E. Domine, S. Valencia

Water-resistant solid Lewis acid catalysts: Meerwein-Ponndorf-Verley and Oppenauer reactions catalyzed by tin-beta zeolite

J. Catal. 215 (2003) 294–304.

[34] A. Corma, M. E. Domine, L. Nemeth, S. Valencia

Al-Free Sn-Beta Zeolite as a Catalyst for the selective reduction of carbonyl compounds (Meerwein–Ponndorf–Verley Reaction)

J. Am. Chem. Soc. 124 (2002) 3194–3195.

[35] H.Y. Luo, D.F. Consoli, W.R. Gunther, Y. Román-Leshkov

Investigation of the reaction kinetics of isolated Lewis acid sites in Beta zeolites for the Meerwein–Ponndorf–Verley reduction of methyl levulinate to γ-valerolactone

J. Catal. 320 (2014) 198–207.

[36] M. Boronat, A. Corma, M. Renz, P.M. Viruela

Predicting the activity of single isolated Lewis acid sites in solid catalysts

Chem. - A Eur. J. 12 (2006) 7067–7077.

[37] R.F. Perez, M.A. Fraga

Hemicellulose-derived chemicals: one-step production of furfuryl alcohol from xylose

Green Chem. 16 (2014) 3942–3950.

[38] R.F. Perez, O.S.G.P. Soares, A.M.D. de Farias, M.F.R. Pereira, M.A. Fraga

Conversion of hemicellulose-derived pentoses over noble metal supported on 1D multiwalled carbon nanotubes

Appl. Catal. B Environ. 232 (2018) 101–107.

[39] R.F. Perez, S.J. Canhaci, L.E.P. Borges, M.A. Fraga

One-step conversion of xylose to furfuryl alcohol on sulfated zirconia-supported Pt catalyst—Balance between acid and metal sites

Catal. Today. 289 (2017) 273–279.

[40] S.J. Canhaci, R.F. Perez, L.E.P. Borges, M.A. Fraga,

Direct conversion of xylose to furfuryl alcohol on single organic–inorganic hybrid mesoporous silica-supported catalysts

Appl. Catal. B Environ. 207 (2017) 279–285.

[41] P.N. Paulino, R.F. Perez, N.G. Figueiredo, M.A. Fraga

Tandem dehydration–transfer hydrogenation reactions of xylose to furfuryl alcohol over zeolite catalysts

Green Chem. 19 (2017) 3759–3763.

[42] R.F. Perez, E.M. Albuquerque, L.E.P. Borges, C. Hardacre, M.A. Fraga

Aqueous-phase tandem catalytic conversion of xylose to furfuryl alcohol over [Al]-SBA-15 molecular sieves

Catal. Sci. Technol. 9 (2019) 5350–5358.

[43] J. Iglesias, J.A. Melero, G. Morales, J. Moreno, Y. Segura, M. Paniagua, A. Cambra, B. Hernández

Zr-SBA-15 Lewis acid catalyst: Activity in Meerwein Ponndorf Verley reduction

Catalysts. 5 (2015) 1911–1927.

[44] J. Hidalgo-Carrillo, A. Parejas, M.J. Cuesta-Rioboo, A. Marinas, F.J. Urbano

MPV Reduction of furfural to furfuryl alcohol on Mg, Zr, Ti, Zr–Ti, and Mg–Ti solids: Influence of acid–base properties

Catalysts 8 (2018).

[45] C.A. Emeis

Determination of integrated molar extinction coefficients for infrared absorption bands of pyridine adsorbed on solid acid catalysts

J. Catal. 141 (1993) 347–354.

[46] G. Li, L. Gao, Z. Sheng, Y. Zhan, C. Zhang, J. Ju, Y. Zhang, Y. Tang

A Zr-Al-Beta zeolite with open Zr(iv) sites: an efficient bifunctional Lewis–Brønsted acid catalyst for a cascade reaction

Catal. Sci. Technol. 9 (2019) 4055–4065.

[47] H.P. Winoto, Z.A. Fikri, J.M. Ha, Y.K. Park, H. Lee, D.J. Suh, J. Jae

Heteropolyacid supported on Zr-Beta zeolite as an active catalyst for one-pot transformation of furfural to γ-valerolactone

Appl. Catal. B Environ. 241 (2019) 588–597.

[48] R. Hajjar, Y. Millot, P. P. Man, M. Che, S. Dzwigaj

Two kinds of framework Al Sites studied in BEA zeolite by X-ray diffraction, Fourier transform infrared spectroscopy, NMR techniques, and V probe

J. Phys. Chem. C. 112 (2008) 20167–20175.

[49] E. Fernández López, V. Sánchez Escribano, M. Panizza, M.M. Carnasciali, G. Busca

Vibrational and electronic spectroscopic properties of zirconia powders

J. Mater. Chem. 11 (2001) 1891–1897.

[50] B. Tang, W. Dai, X. Sun, G. Wu, N. Guan, M. Hunger, L. Li

Mesoporous Zr-Beta zeolites prepared by a post-synthetic strategy as a robust Lewis acid catalyst for the ring-opening aminolysis of epoxides

Green Chem. 17 (2015) 1744–1755.

[51] P. Wolf, C. Hammond, S. Conrad, I. Hermans

Post-synthetic preparation of Sn-, Ti- and Zr-beta: a facile route to water tolerant, highly active Lewis acidic zeolites

Dalt. Trans. 43 (2014) 4514–4519.

[52] J. El Haskouri, S. Cabrera, C. Guillem, J. Latorre, A. Beltrán, D. Beltrán, M. Dolores Marcos, P. Amorós

Atrane precursors in the one-pot surfactant-assisted synthesis of high zirconium content porous silicas

Chem. Mater. 14 (2002) 5015–5022.

[53] A. Janin, M. Maache, J.C. Lavalley, J.F. Joly, F. Raatz, N. Szydlowski

FT i.r. study of the silanol groups in dealuminated HY zeolites: Nature of the extraframework debris

Zeolites. 11 (1991) 391–396.

[54] S. Dzwigaj, P. Massiani, A. Davidson, M. Che

Role of silanol groups in the incorporation of V in β zeolite

J. Mol. Catal. A Chem. 155 (2000) 169–182.

[55] K. Chakarova, K. Hadjiivanov

H-bonding of zeolite hydroxyls with weak bases: FTIR study of CO and N_2 adsorption on H-D-ZSM-5

J. Phys. Chem. C. 115 (2011) 4806–4817.

[56] V.L. Sushkevich, I.I. Ivanova

Ag-promoted ZrBEA zeolites obtained by post-synthetic modification for conversion of ethanol to butadiene

ChemSusChem. 9 (2016) 2216–2225.

[57] V. L. Sushkevich, A. Vimont, A. Travert, I. I. Ivanova

Spectroscopic evidence for open and closed lewis acid sites in ZrBEA zeolites

J. Phys. Chem. C. 119 (2015) 17633–17639.

[58] S. Dzwigaj, Y. Millot, J.-M. Krafft, N. Popovych, P. Kyriienko

Incorporation of silver atoms into the vacant T-atom sites of the framework of SiBEA zeolite as mononuclear Ag(I) evidenced by XRD, FTIR, NMR, DR UV–vis, XPS, and TPR

J. Phys. Chem. C. 117 (2013) 12552–12559.

[59] S. Dzwigaj, M. Matsuoka, M. Anpo, M. Che

Effect of metal content and calcination–hydration on the environment of V in zeolites prepared by impregnation of SiBEA with $V^{IV}OSO_4$ solution

Microporous Mesoporous Mater. 93 (2006) 248–253.

[60] K.I. Hadjiivanov, G.N. Vayssilov

Characterization of oxide surfaces and zeolites by carbon monoxide as an IR probe molecule

Adv. Catal. 47 (2002) 307–511.

[61] V. V Ordomsky, V.Y. Murzin, Y.V. Monakhova, Y. V Zubavichus, E.E. Knyazeva, N.S. Nesterenko, I.I. Ivanova

Nature, strength and accessibility of acid sites in micro/mesoporous catalysts obtained by recrystallization of zeolite BEA

Microporous Mesoporous Mater. 105 (2007) 101–110.

[62] S. Dzwigaj, E. Ivanova, R. Kefirov, K. Hadjiivanov, F. Averseng, J.M. Krafft, M. Che **Remarkable effect of the preparation method on the state of vanadium in BEA zeolite: Lattice and extra-lattice V species**

Catal. Today. 142 (2009) 185–191.

[63] V. Choudhary, A.B. Pinar, S.I. Sandler, D.G. Vlachos, R.F. Lobo **Xylose isomerization to xylulose and its dehydration to furfural in aqueous media**

ACS Catal. 1 (2011) 1724–1728.

Figure 1. DR UV-Vis spectra of all zeolite samples.

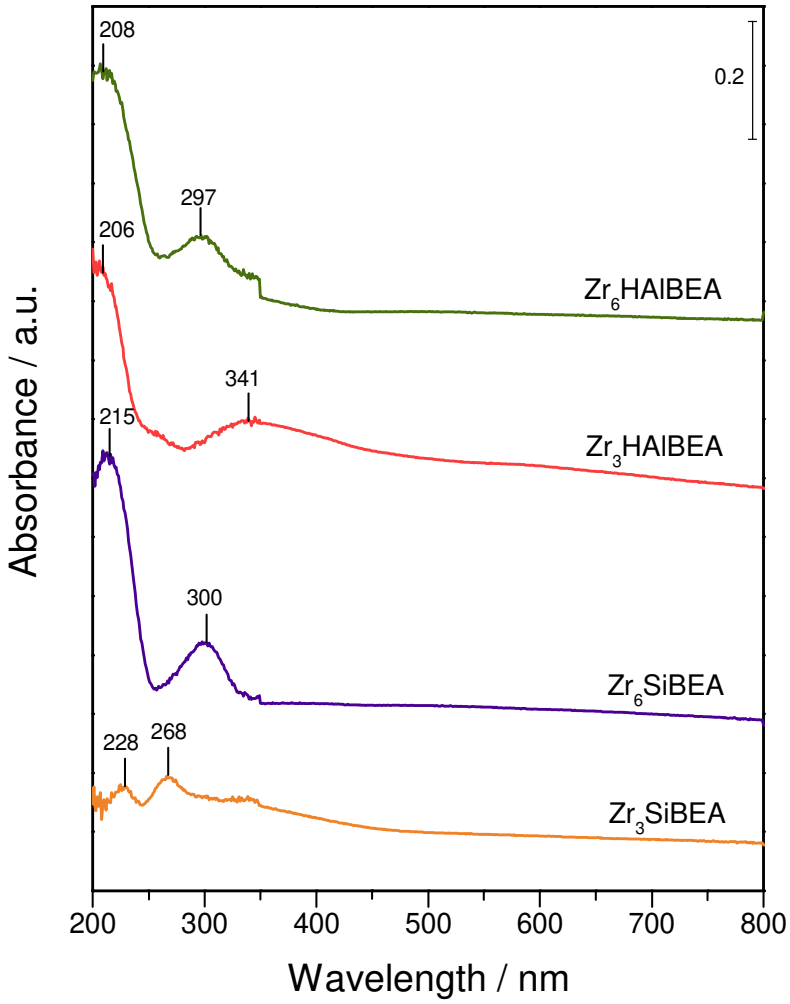

Figure 2. Infrared spectra of HAlBEA and Zr_6HAlBEA, and SiBEA and Zr_6SiBEA, in the range of OH vibrating modes, at -173 °C, before CO adsorption.

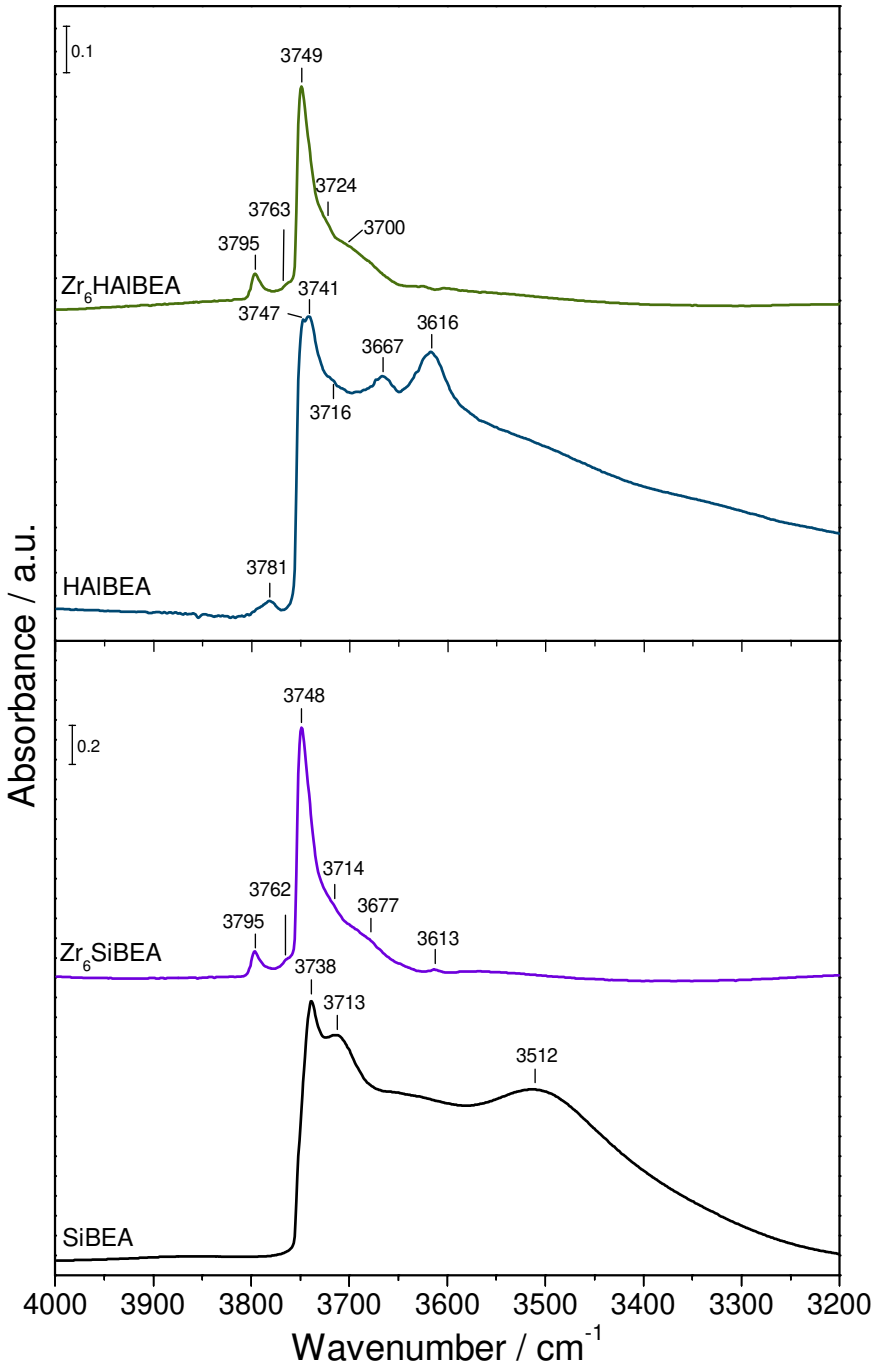

Figure 3. Infrared spectra of pyridine adsorbed on SiBEA, Zr_3SiBEA, Zr_6SiBEA, HAlBEA, Zr_3HAlBEA and Zr_6HAlBEA, in the range of 1700-1400 cm^{-1}.

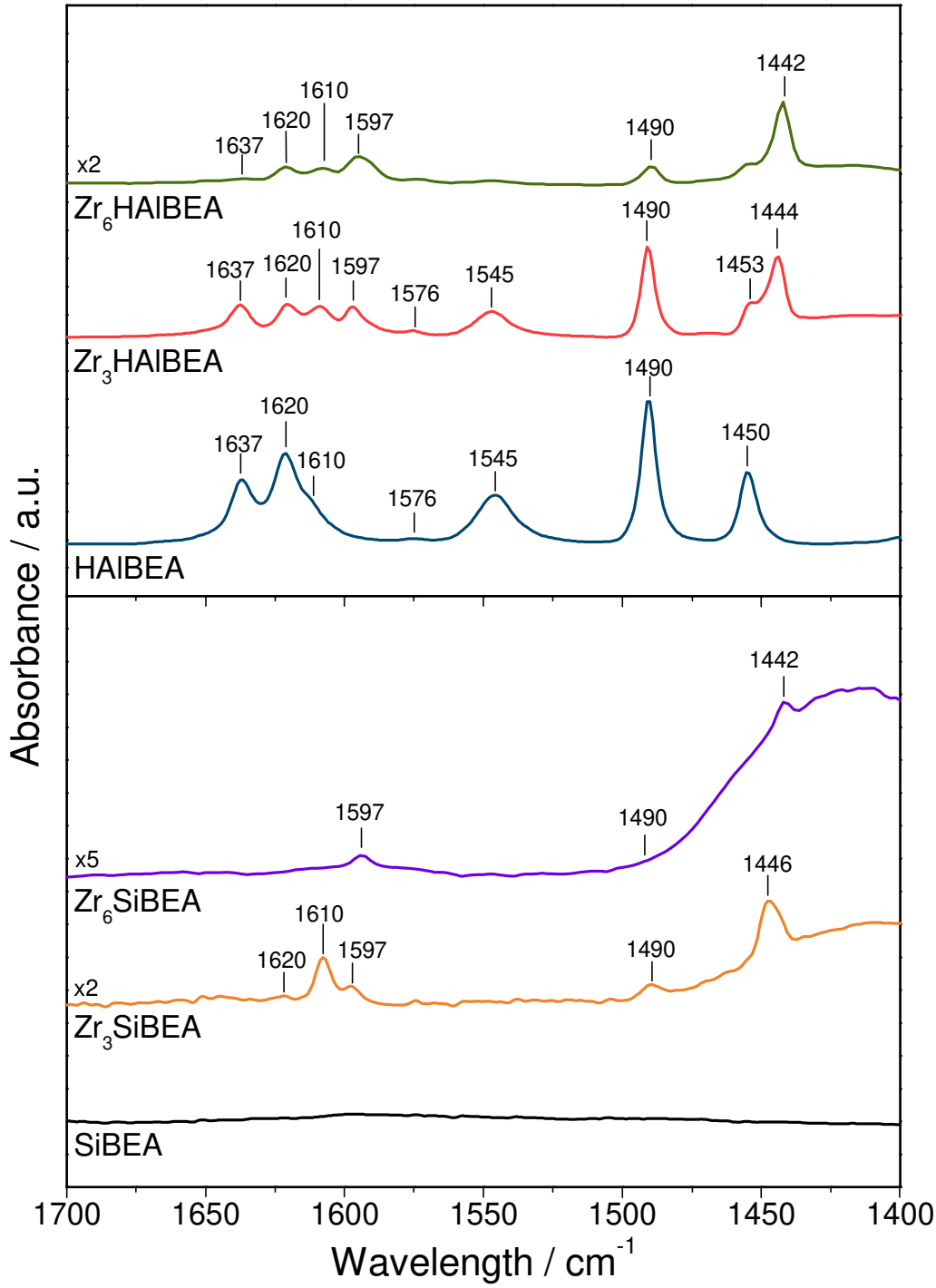

Figure 4. Infrared spectra in the OH vibrating modes range of CO adsorption on HAlBEA, Zr_6HAlBEA, SiBEA and Zr_6SiBEA at -173 °C, CO equilibrium pressure of 100 Pa and the development of spectra during evacuation (b-f).

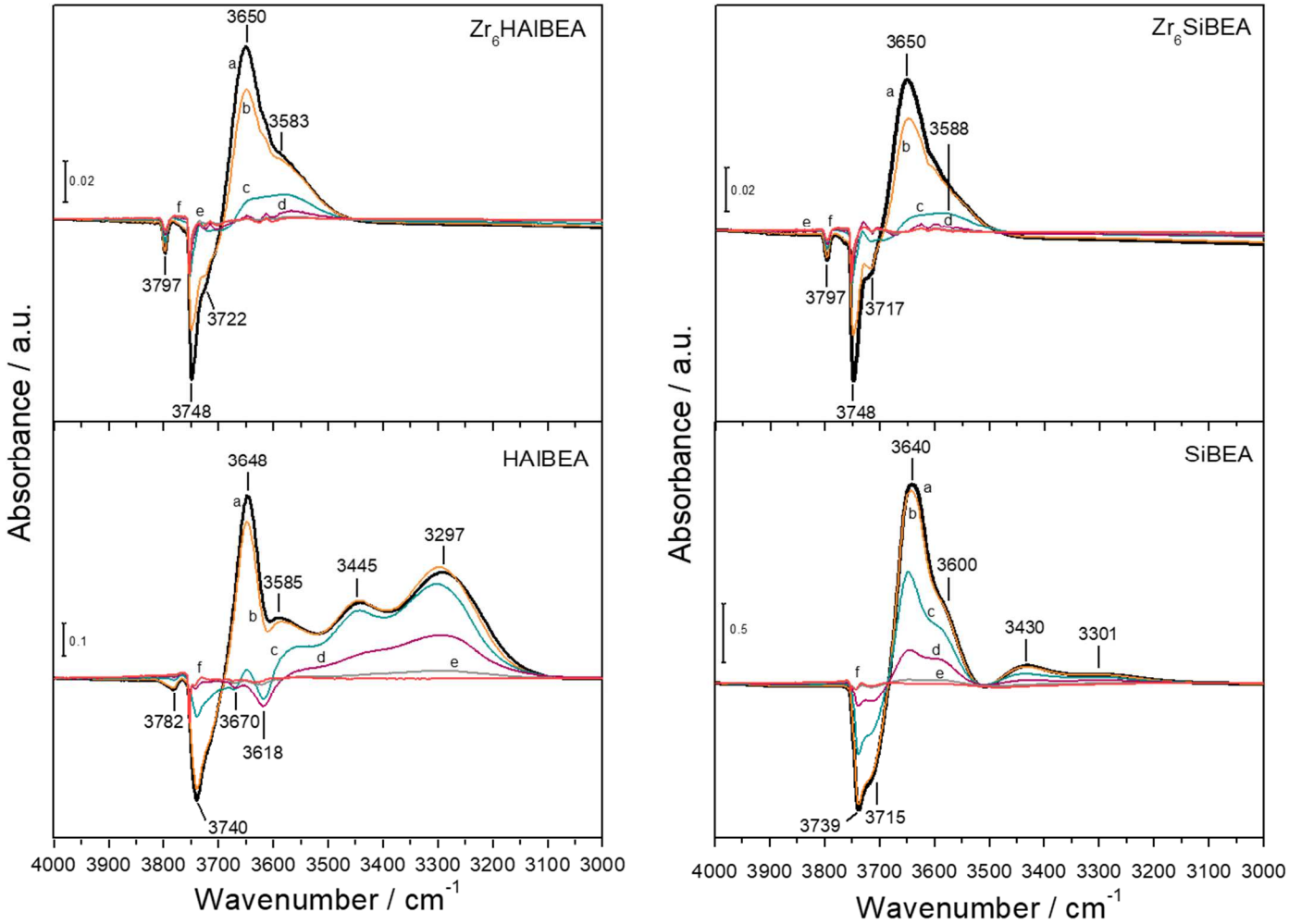

Figure 5. Infrared spectra in the carbonyl stretching modes range of CO adsorption on HAlBEA, Zr_6HAlBEA, SiBEA and Zr_6SiBEA at -173 °C, CO equilibrium pressure of 100 Pa, and the development of spectra during evacuation (b-f).

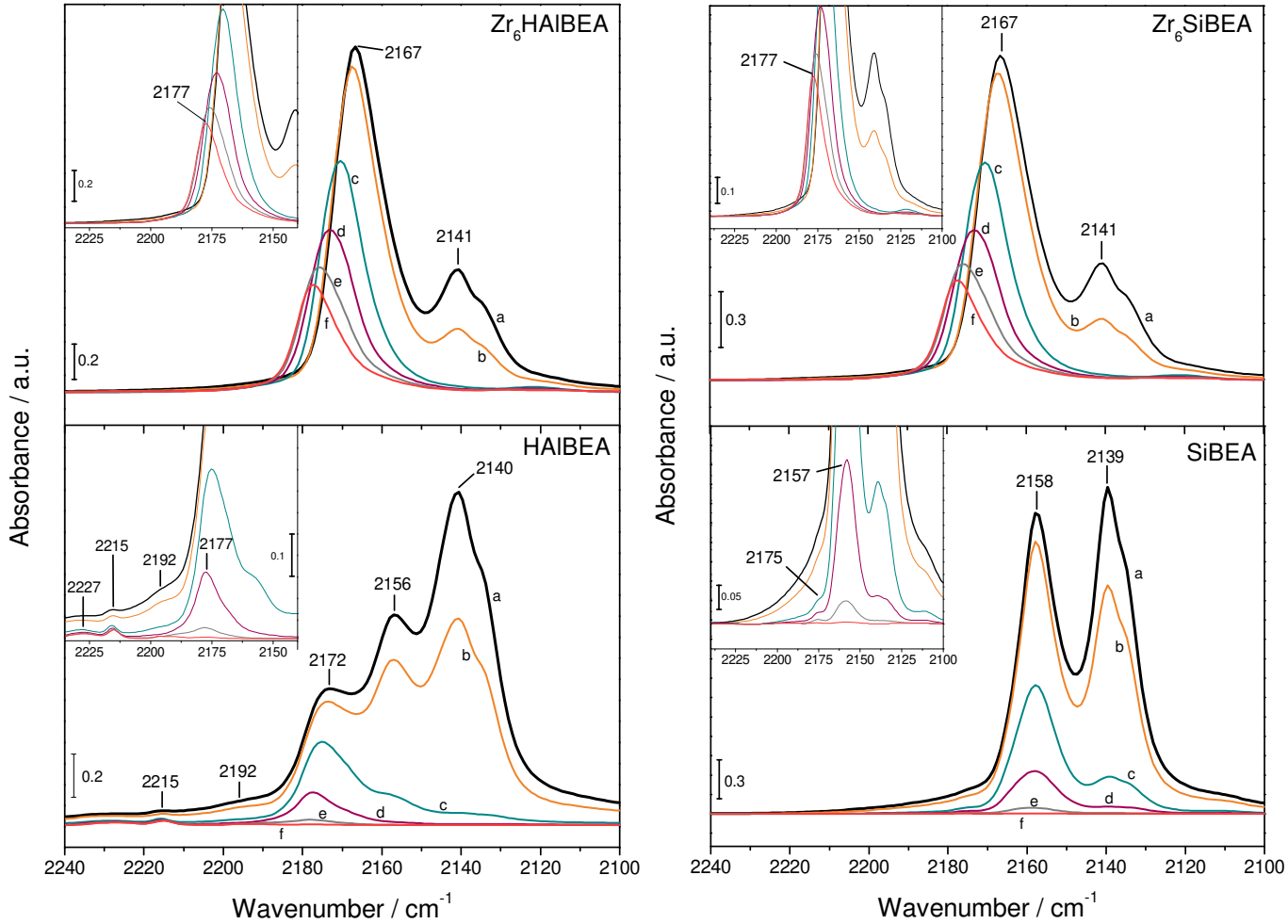

Figure 6. Xylose conversion curves as a function of reaction time on (▲) SiBEA, ( ) Zr_3SiBEA, (⬢) Zr_6SiBEA, (□) HAlBEA, (●) Zr_3HAlBEA, (△) Zr_6HAlBEA. Reaction condition: xylose solution at 83 mmol L^{-1}, water:isopropanol 1:1, temperature 130 °C, 30 bar (N_2).

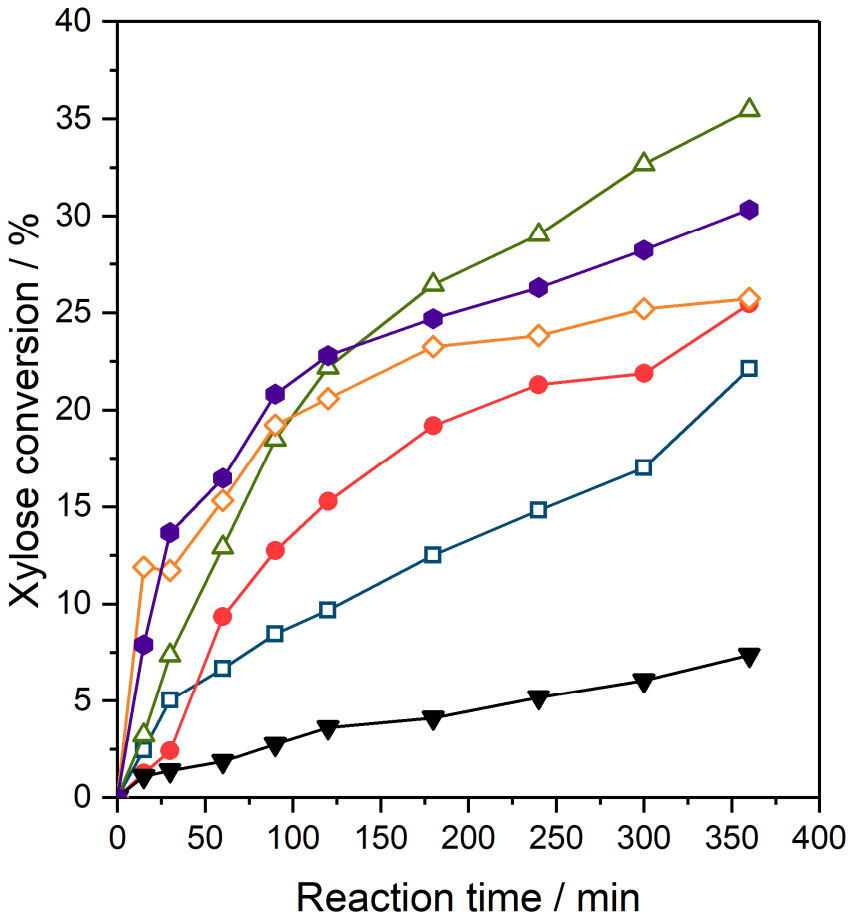

Figure 7. Selectivities to (▶) xylulose, (▷) furfuryl alcohol, (▶) furfural and (✳) carbon balance over (a) Zr_3SiBEA and (b) Zr_6SiBEA catalysts. Reaction condition: xylose solution at 83 mmol L^{-1}, water:isopropanol 1:1, temperature 130 °C, 30 bar (N_2).

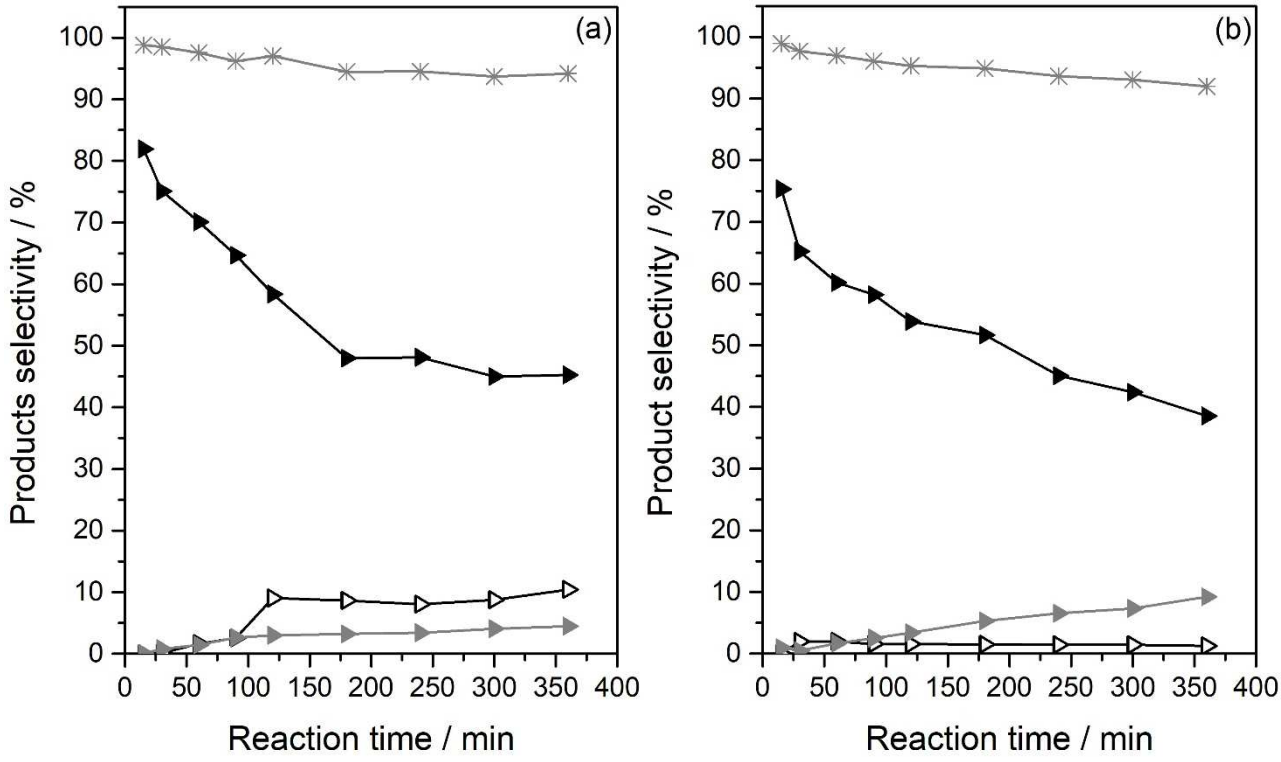

Figure 8. Selectivities to (▶) xylulose, (▷) furfuryl alcohol, (▶) furfural and (✳) carbon balance over (a) HAlBEA, (b) Zr_3HAlBEA and (c) Zr_6HAlBEA catalysts. Reaction condition: xylose solution at 83 mmol L^{-1}, water:isopropanol 1:1, temperature 130 °C, 30 bar (N_2).

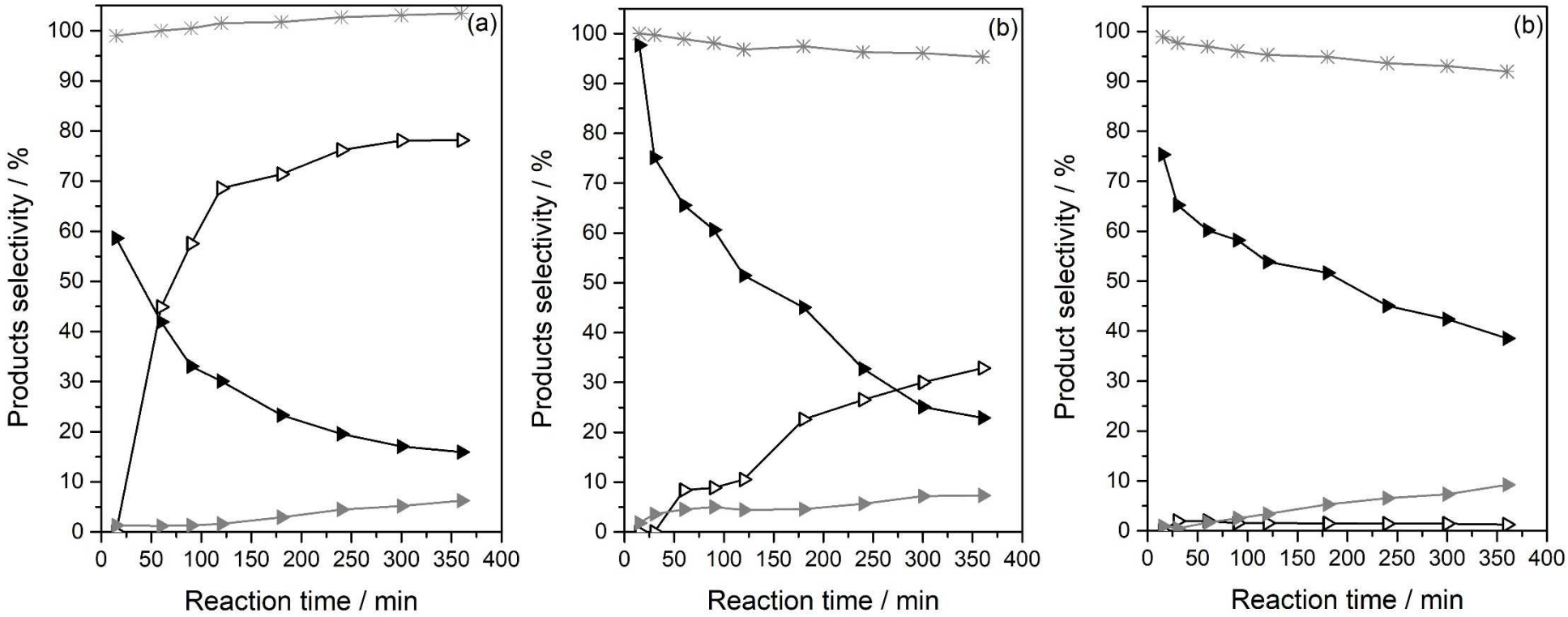

Figure 9. Xylose conversion and selectivities to xylulose, furfuryl alcohol and furfural for three consecutive reaction cycles performed using Zr_3HAlBEA. Reaction condition: xylose solution at 83 mmol L^{-1}, water:isopropanol 1:1, temperature 130 °C, 30 bar (N_2), 6 h of reaction.

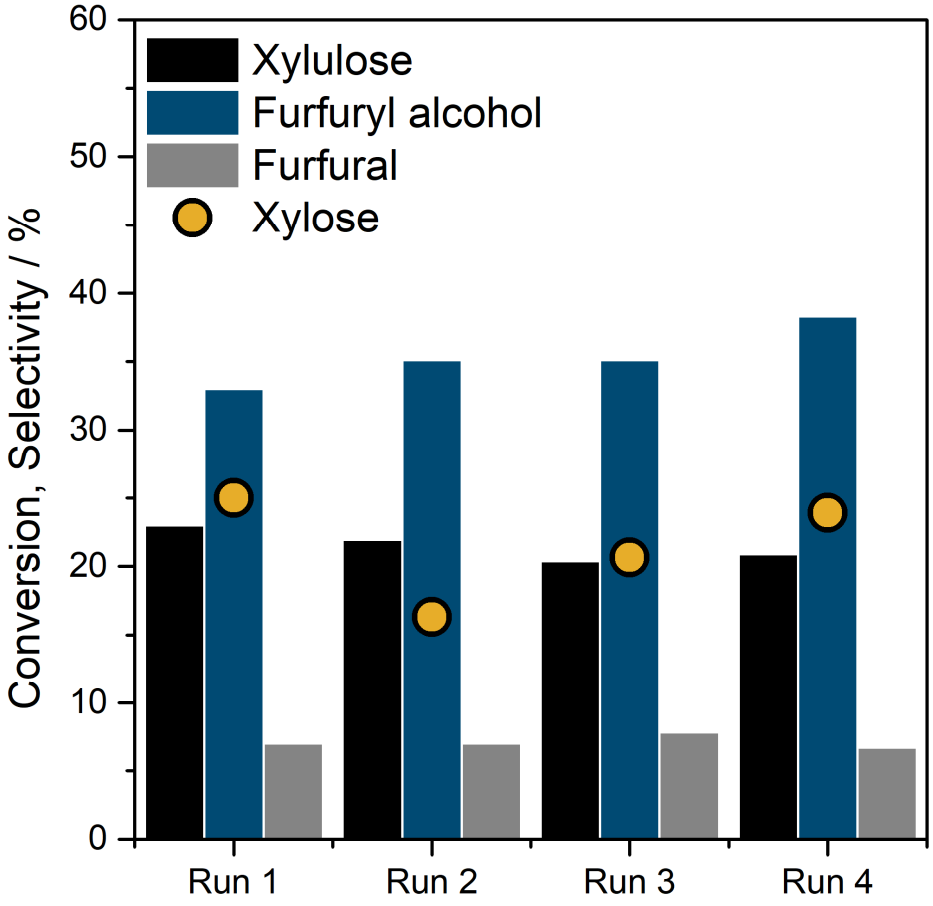

Scheme 1. Simplified reaction scheme of xylose conversion into furfuryl alcohol.

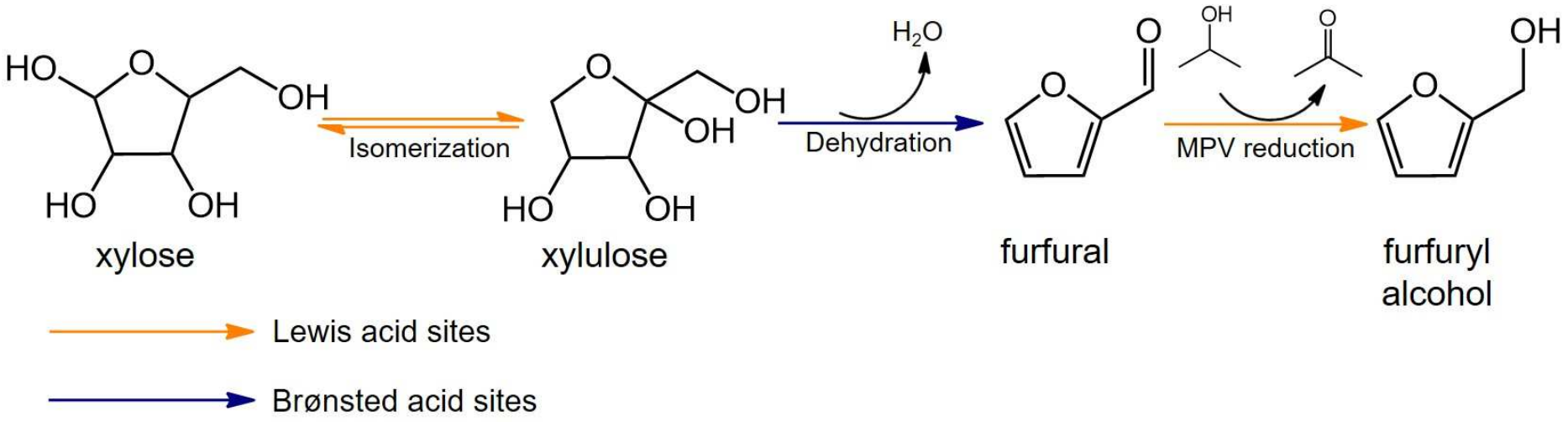

Table 1. Aluminium (% Al) and zirconium content (% Zr), Si/Al and Si/Zr ratios, surface area (S_{BET}) and concentration of Brønsted (BAS) and Lewis (LAS) acid sites.

Catalyst	Al (wt%)	Si/Al	Zr (wt%)	Si/Zr	S_{BET} (m^2 g^{-1})	BAS (µmol g^{-1})	LAS (µmol g^{-1})
SiBEA	-	1000	-	-	610	-	-
Zr_3SiBEA	-	1000	3.2	51	413	-	20
Zr_6SiBEA	-	1000	5.7	23	445	-	-
HAlBEA	3.0	14	-	-	569	219	114
Zr_3HAlBEA	2.9	14	3.2	50	515	156	71
Zr_6HAlBEA	3.0	14	6.3	22	466	6	61

Graphical Abstract